Laser Physics, Vol. 15, No. 9, 2005, pp. 1319-1333.

Study of Broadband Optical Parametric Chirped Pulse Amplification in a DKDP Crystal Pumped by the Second Harmonic of a Nd:YLF Laser

V. V. Lozhkarev, G. I. Freidman, V. N. Ginzburg, E. A. Khazanov*, O. V. Palashov, A. M. Sergeev, and I. V. Yakovlev

Institute of Applied Physics, Russian Academy of Sciences, Nizhni Novgorod, 603950 Russia
*e-mail: khazanov@appl.sci-nnov.ru
Received December 27, 2004

Abstract - The validity of data on the Sellmeier equation [Kirby K. W. DeShazer L. G., JOSA B, **4,** 1072- 1078 (1987)] modified by linearly approximating the dependence of the linear susceptibility on the deuteration level has been verified experimentally. Conditions for broadband optical parametric amplification of chirped pulses in a DKDP crystal at a pump wavelength of 527 nm have been investigated. It is shown that the DKDP crystal is more suitable than the KDP crystal for powerful OPCPA stages in petawatt lasers. Based on a Cr:forsterite laser and optical parametric amplification in the DKDP crystal, a laser with 0.4-TW power at a wavelength of 911 nm has been developed.

INTRODUCTION

Optical parametric chirped pulse amplification (OPCPA) is currently being extensively investigated as a promising way to overcome the petawatt power barrier. The OPCPA systems employ the traditional method of superstrong field generation, i.e., stretching of short light pulses (frequency modulation), multistage amplification of their energy, and subsequent recompression of the amplified pulses. Conditions for broadband phase matching can be achieved by appropriately choosing an amplifying nonlinear medium and the frequencies and propagation directions of interacting waves in OPA stages [1-15].

The second harmonic of Nd:glass lasers with a wavelength of 527 nm is most promising for pumping powerful optical parametric amplifiers. At this pumping, the best candidates for the optical parametric amplifying medium are LBO, BBO, KDP, and DKDP nonlinear crystals. The former two crystals have strong nonlinearity; however, current crystal growth technology cannot provide LBO and BBO crystals with large transverse dimensions. As a result, these crystals can be used only in the first OPA stages. KDP and DKDP crystals, although they exhibit a weaker nonlinearity, can be grown to an aperture of 30 cm and more; see, for example, [16]. This enables them to be used in the final stages of optical parametric amplifiers of at the petawatt power level.

In almost all works dedicated to the creation of optical parametric amplifiers of femtosecond pulses up to multiterawatt and petawatt power levels, the nonlinear elements for final OPA stages were made of KDP crystal [3, 4, 6, 17]. At the same time, little attention has been given to its isomorph—the DKDP crystal. Here, we shall show that the ultrabroadband phase-matching conditions could be fulfilled in this crystal upon noncollinear nondegenerate interaction and that, in this case, the gain band is more than twice as broad as that in KDP.

Knowledge of the dispersion dependences of the refractive index and their derivatives is essential for studying nonlinear crystal properties and optimal broadband parametric interaction conditions. Meanwhile, our analysis of data reported in the literature [18-23] shows that, in the 850-1300-nm wavelength range of interest, the dispersion characteristics of DKDP crystals with a high deuteration level have not been very thoroughly investigated. Specifically, two Sellmeier equations presented in the well-known handbook [24] give significantly different values of optimal parameters for broadband amplification.

In Section 1, we present the results of our analysis of the dispersion characteristics of DKDP crystals, which allowed us to draw a conclusion concerning the most reliable Sellmeier equation for this crystal. We also discuss the effect of the DKDP deuteration level on broadband gain characteristics.

The experimental study of OPCPA based on the DKDP crystal is discussed in Section 2. We also report experimental results supporting our theoretical analysis of broadband optical parametric chirped pulse amplification in highly deuterated DKDP crystals pumped by the second harmonic of a Nd:YLF laser.

In Section 3, we describe a femtosecond laser developed on the basis of OPCPA in a DKDP crystal, which serves as a front-end system for the petawatt laser currently under construction.

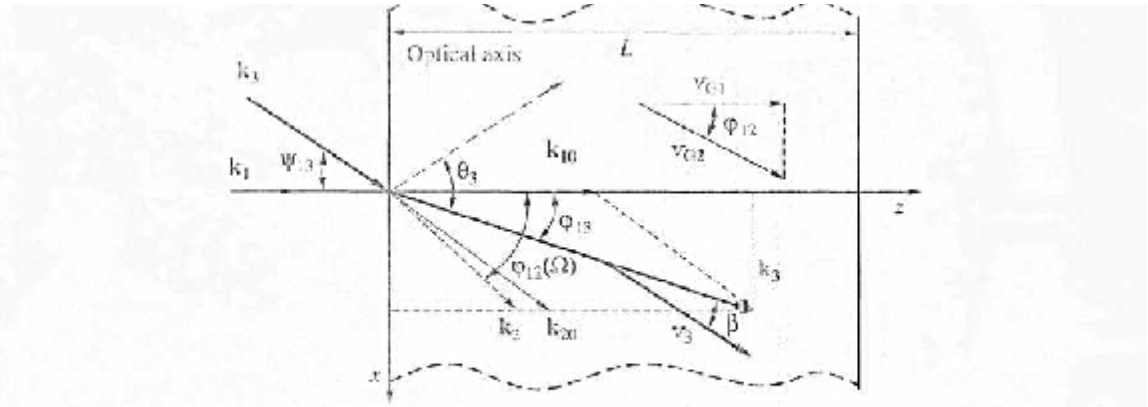

Fig. 1. Schematic diagram of noncollinear three-wave type I interaction (oo–e) in a nonlinear crystal at optical parametric amplification of broadband signal radiation.

1. THEORETICAL ANALYSIS OF BROADBAND OPCPA

1.1. Phase Matching, Broadband Phase Matching, and Ultrabroadband Phase Matching at Noncollinear Nondegenerate Parametric Interaction.

Broadband amplification is generally studied by analyzing conditions of broadband phase matching in a nonlinear crystal and calculating dispersion characteristics and spectral angular dependences of interacting waves. The parametric gain band in a nonlinear crystal is determined by the wavevector mismatch between interacting waves $\Delta k(\Omega)$. Unsaturated gain with respect to photon number in the signal wave is given by the following well-known formula:

$$G = 1 + (\gamma L)^2 \left(\frac{\sinh BL}{BL}\right)^2. \qquad (1)$$

Here, $B = \sqrt{q^2 - (\Delta k/2)^2}$; $\gamma = \chi_2 (I_3)^{1/2}$ is the wave interaction coefficient; $\chi_2 = 4\pi d_{\text{eff}}(2\varepsilon_0 n_1 n_2 n_3 c\lambda_1\lambda_2)^{-1/2}$ is the quadratic nonlinearity coefficient; I_3 is the intensity of pump radiation; L is the length of the nonlinear element; and d_{eff} is the effective nonlinearity, an expression for which is determined by the crystal symmetry and angles between the crystallographic axes and the phase-matching directions [24]:

$$d_{\text{eff}} = d_{36}\sin\theta_3 \sin 2\phi \quad \text{for KDP and DKDP crystals,}$$

$$d_{\text{eff}} = d_{31}\sin\theta_3 - d_{22}\cos\theta_3 \sin 3\phi \quad \text{for a BBO crystal,}$$

where d_{ij} are coefficients of the matrix of nonlinear optical susceptibility.

As one can see from (1), if $\Delta k(\Omega)$ grows, the value of the gain coefficient G decreases. Therefore, the study of broadband optical parametric amplification consists in determining the phase-matching conditions at which the value of $\Delta\mathbf{k}(\Omega)$ would be minimal and, hence, signal radiation would be amplified in the maximum possible frequency band.

Let us consider optical parametric amplification of broadband radiation in a nonlinear crystal whose continuous frequency spectrum may be represented as $\omega_1 = \omega_{10} + \Omega$. The schematic diagram of the noncollinear three-wave interaction is illustrated in Fig. 1. Here and further throughout the text, we shall consider type 1 (oo-e) phase matching. Let wavevectors $\mathbf{k}_1(\omega_1)$ of the signal radiation injected into the nonlinear crystal *(o* wave) be directed along the z axis, perpendicular to the input surface of the nonlinear crystal. The wavevector of the collimated monochromatic pump radiation *(e* wave) $\mathbf{k}_3(\omega_3)$ is directed inside the crystal relative to the z axis at an angle φ_{13}. In this case, it follows from the boundary conditions that the x-components of the idler wavevectors will be equal to a corresponding component of the pump wavevector:

$$k_{2x}(\omega_2) = k_{3x}, \qquad (2)$$

where $\omega_2 = \omega_{20} - \Omega$ In contrast to the signal wave, the idler wave has an angular spectrum of wavevectors $k_2(\omega_2)$. Indeed, each frequency ω_2 has its corresponding angle $\varphi_{12}(\omega_2)$ between the wavevector $k_2(\omega_2)$ and the z axis, which is determined by the expression

$$\cos\phi_{12}(\omega_2) = k_{2z}(\omega_2)/k_2(\omega_2),$$

$$\text{where} \quad k_{2z}(\omega_2) = \sqrt{k_2^2(\omega_2) - k_{2x}^2}.$$

By virtue of relation (2), the wavevector mismatch $\Delta\mathbf{k}(\Omega)$ is directed along the z axis. The Taylor scries

expansion of the wavevector mismatch around the central frequency has the form

$$\Delta k(\Omega) = \Delta k_0 - \left(\frac{dk_1}{d\omega_1} - \frac{dk_{2s}}{d\omega_2}\right)\Omega - \frac{1}{2}\left(\frac{d^2k_1}{d\omega_1^2} - \frac{d^2k_{2s}}{d\omega_2^2}\right)\Omega^2 + \ldots, \quad (3)$$

where $\Delta k_0 = k_3(\omega_3) - k_1(\omega_{10}) - k_2(\omega_{20})\cos(\varphi_{12})$ is the wavevector mismatch at the central frequencies and $\varphi_{12} = \varphi_{12}(\Omega = 0)$ is the angle at a central frequency. By analyzing expression (3) for the wavevector mismatch $\Delta k(\Omega)$, we can obtain the necessary conditions for optical parametric amplification of broadband radiation.

We shall call the phase matching "broadband" if, simultaneously with the phase-matching condition at the central frequencies

$$\Delta k_0 = 0, \quad (4)$$

the condition at which the second component in expression (3) becomes zero is fulfilled:

$$V_{G1}(\omega_{10}) = V_{G2}(\omega_{20})\cos\varphi_{12}, \quad (5)$$

where $V_{Gi}(\omega_{i0}) = d\omega_i/dk_i$ is the group velocity of the signal (idler) wave. Here, $\Delta k(\Omega)$ depends only on terms quadratic in Ω and higher order terms. Broadband phase matching can be obtained in any nonlinear crystal in which the phase-matching conditions are satisfied for a range of signal wavelengths determined by the following condition:

$$V_{G1}(\lambda_{10}) \le V_{G2}(\lambda_{20}).$$

In particular, the broadband phase-matching condition is automatically fulfilled for degenerate ($\lambda_{10} = \lambda_{20}$) collinear type 1 interaction when the group velocities of the signal and idler waves arc collinear and equal. Hereinafter, we shall use the term "signal radiation" with regard to a wave with a lower group velocity $V_{GS}(\lambda_{10}) \le V_{GI}(\lambda_{20})$, in contrast to the works in which short-wave radiation $\omega_s > \omega_i$ was termed signal radiation (see, e.g., [3]).

We shall use the term ultrabroadband phase matching when, simultaneously with broadband phase-matching conditions (4-5), the condition at which the third component in expression (3) becomes zero is satisfied:

$$\frac{d^2k_1}{d\omega_1^2} + \frac{1}{\cos\varphi_{12}}\frac{d^2k_2}{d\omega_2^2} - \frac{1}{V_{G2}^2 k_{20}\cos\varphi_{12}}\tan^2\varphi_{12} = 0. \quad (6)$$

Here, the wavevector mismatch $\Delta k(\Omega)$ is determined by a term that is cubic in Ω and by higher order terms.

For a particular nonlinear crystal and a predetermined pump wavelength, there are three free parameters: the signal (or idler) wavelength and two independent angles between the wavevector directions and the crystal's optical axis. However, three nonlinear equations (Eqs. (4)-(6)) with three unknowns do not always have a solution.

To answer the question of the existence of ultrabroadband phase matching, as can be seen from expression (3), it is necessary and sufficient to know only the dispersion dependences for a particular crystal. The second derivatives of the refractive index are most sensitive to constants and the form of the Sellmeier dispersion relations. Moreover, the group velocity dispersion determines the gain bandwidth at broadband phase matching (see formulas (1) and (3)).

There is a parameter that helps define the wavelength range of the pump and the signal at which the gain bandwidth is maximal. As we will show below, this parameter is a wavelength $\lambda^* = 2\pi c/\omega^*$, at which the second derivative of the wave number of an ordinary wave becomes zero:

$$\frac{d^2k}{d\omega^2}(\omega^*) = 0. \quad (7)$$

We shall call this wavelength a critical wavelength λ^*.

1.2. Analysis of Published Sellmeier Equations for a DKDP Crystal

An analysis of three different Sellmeier equations for a KDP crystal reported in [18, 25, 26] shows that they coincide with a fairly good accuracy over a broad spectral range [24, 27]. Figure 2 illustrates the dependences of refractive indexes and wavevector derivatives with respect to frequency $dk/d\omega$ and $d^2k/d\omega^2$ for ordinary and extraordinary waves in DKDP crystals [18-23]. Additionally, the Sellmeier equation for the KDP crystal is given in this figure for comparison [26]. As can be seen from Fig. 2, the dispersion characteristics of DKDP crystals taken from different sources provide greatly differing values of group velocities and their derivatives. The angles of interaction and, more importantly, values of the critical wavelength λ^* also turn out to be different.

Figure 2a shows the nonphysical behavior of curve *4* [21] for an ordinary wave in the long-wave range: according to it, the refractive index increases with increasing wavelength. This is apparently due to improper choice of the resonance term introduced in [21]. Dispersion dependences of group velocities for curves *2* and *3* (Fig. 2b, 2c) sharply distinguish them from other curves. This also raises doubts about their correctness. Curve 5 [22] was obtained from the Sellmeier equation for KDP crystal by adding an additive that is linear both in DKDP deuteration level and in wavelength. Therefore, values for the group velocity

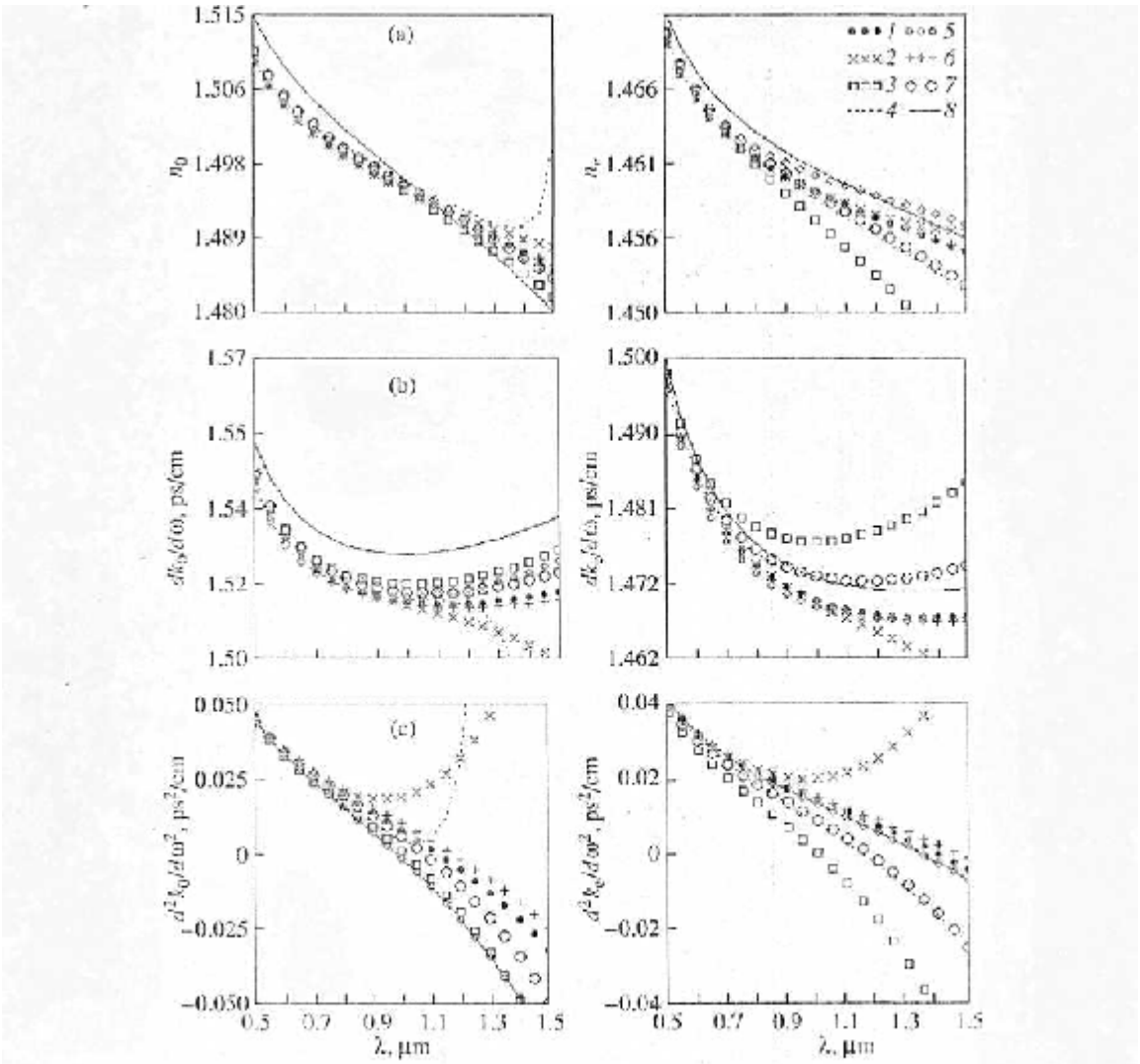

Fig. 2. Values of refractive indices n_o and n_e and their derivatives for DKDP crystal: *1*—[18] (modified), *2*—[23], *3*—[20], *4*—[21], *5*—[22], *6*—[18] (standard), *7*—[19], *8*—Sellmeier equation for KDP crystal [26].

dispersion of curve *5* are strictly equal to those for KDP 8, which docs not correspond to the dispersion characteristics of highly deuterated DKDP crystals (see [18]). Curve 7 was obtained for the wavelength range of 400-690 nm and cannot with reliable accuracy describe the dispersion characteristics beyond this range.

Handbook [24] gives references to two Sellmeier equations for DKDP crystals—curves *1* [18] and *3* [20]—stating that curve *1* provides a better approximation, while curve *3* is temperature-dependent. Curves *6* and *1* are very close in all figures. They were compared in [18] and clear preference was given to the equation corresponding to curve *1*. The validity of dispersion characteristic (1) is also supported by the results of [27], in which the characteristics of noncritical phase matching at second-harmonic generation in partially deuterated (up to 40%) KDP crystals were studied.

The Sellmeier formulas from [18] were obtained for crystals with a high deuteration level, namely, 96%, and do not allow one to judge the effect of the deuteration level of the DKDP crystal on the parametric interaction characteristics. Note that the validity range reported in this work lies within 404.6-1064-nm wavelengths. Therefore, data from [27] also need to be verified experimentally.

Table 1

Sellmeier equation	Kirby modified [18] (9)			Kirby standard [18]			Experiment	
Deuteration level, %	96	89	84	96	89	84	89 ± 0.5	84 ± 2
Internal angle between pump wavevector and crystal axis θ_3, deg	37.03	37.30	37.50	37.24	37.50	37.68	37.3 ± 0.5	–
Internal angle between wavevectors of signal and pump waves φ_{13}, deg	0.91	0.80	0.71	1.19	1.09	1.01	0.79 ± 0.02	0.68 ± 0.05
Internal angle between wavevectors of signal and idler waves φ_{12}, deg	2.16	1.90	1.68	2.83	2.58	2.39	1.89 ± 0.04	1.6 ± 0.1
Angular dispersion of the idler wave $d\Psi_2/d\lambda$, angl. deg/μm	2.58	2.26	2.0	3.37	3.08	2.85	2.17 ± 0.2	–
Angle between group velocities of the signal and pump β_{13}, deg	1.46	1.47	1.48	1.46	1.47	1.48	–	–
$\theta_3 - \theta_{SHG}$, deg, where θ_{SHG} is the phase-matching angle for collinear doubling	0.32	0.24	0.19	0.55	0.46	0.39	–	0.2 ± 0.05
Critical wavelength λ^*, nm	1120	1110	1100	1170	1150	1130	–	–

According to [27], the dependence of the refractive Index of the DKDP crystal on the deuteration level D can be written in the form

$$N^2_{o,e}(D) = N^2_{o,e}(1)D + (1-D)N^2_{o,e}(0). \qquad (8)$$

Using the dispersion characteristics from [18] for DKDP crystal with a deuteration level $D = 0.96$ and from [26] for KDP crystal ($D = 0$), we can write down an expression for the Sellmeier formula at an arbitrary deuteration level D:

$$N^2_{o,e}(D,\lambda) = \left(\frac{N^2_{o,e}(0.96,\lambda) - 0.04N^2_{o,e}(0,\lambda)}{0.96}\right)D + (1-D)N^2_{o,e}(0,\lambda), \qquad (9)$$

where $N^2_{o,e}(0,\lambda)$ and $N^2_{o,e}(0.96,\lambda)$ are defined as

$$N^2_{o,e}(\lambda\ [\mu m]) = A_{o,e} + \frac{B_{o,e}}{\lambda^2 - C_{o,e}} + \frac{F_{o,e}\lambda^2}{\lambda^2 - E_{o,e}},$$

where

Ref.	polarization	A	$B(\times 10^{-3})$	$C(\times 10^{-2})$	F	E
KPD [26]	o	2.259276	10.089562	1.2942625	13.00522	400
$D = 0$	e	2.132668	8.637494	1.2281043	3.2279924	400
DKDP [18] modified	o	2.240921	9.676393	1.5620153	2.2469564	126.920659
$D = 0.96$	e	2.126019	8.578409	1.1991324	0.7844043	123.403402

Our experiments show (see below) that expression (9) provides the best agreement between theoretically calculated and experimentally measured values (see Table 1). We used this expression to study broadband phase-matching characteristics in DKDP crystal.

1.3. Broadband and UltraBroadband Phase Matching in KDP, DKDP, and BBO

By calculating and studying phase-matching characteristics such as wavevector vector mismatch $\Delta k(\Omega)$, spectral dependence of the gain coefficient, and dispersion dependences of phase-matching angles, it is possible to determine, for a given pumping, optimal parameters for broadband amplification in a particular crystal. Our calculations were made using Sellmeier formulas from [26] for KDP; from [181 for DKDP ($D = 0.96$)—see Eq. (9)—and from [28] for BBO.

Figure 3 illustrates the group velocities of ordinary waves for the three nonlinear crystals and group velocities of ordinary conjugated waves versus signal wavelength for various pump wavelengths. The group velocity for an ordinary wave in KDP has a maximum at a wavelength of $\lambda^*_{KDP} = 984$ nm. For pump radiation with a wavelength shorter than $\lambda^*/2 = 492$ nm, the condition $V_{G2} > V_{G1}$ is satisfied m the shortwave region of the signal; i.e., $\lambda_1 < \lambda_2$, whereas, for $\lambda_3 > 492$ nm (in the long-

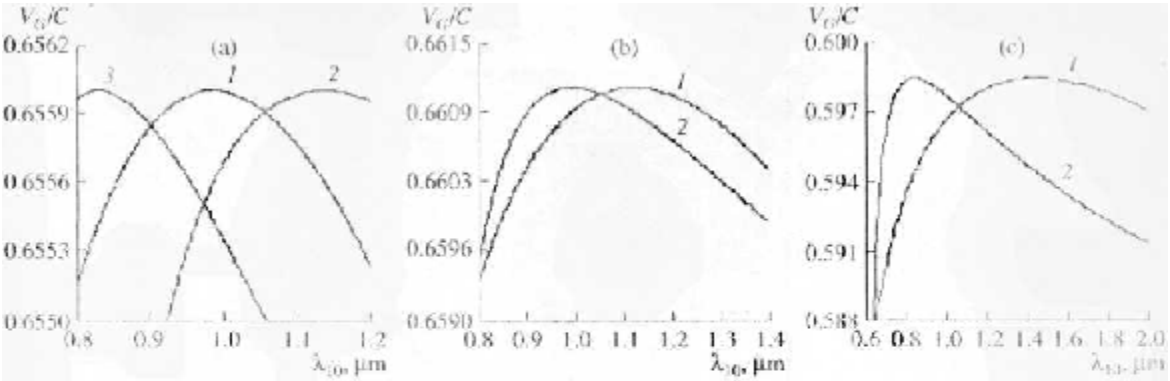

Fig. 3. Group velocity (normalized to light velocity in vacuum) of the *o* wave in KDP (a), DKDP (b) and BBO (c) crystals vs. signal wavelength λ_{10} for *1*—signal wave, *2*—idler wave (527-nm pumping), *3*—idler wave (450-nm pumping).

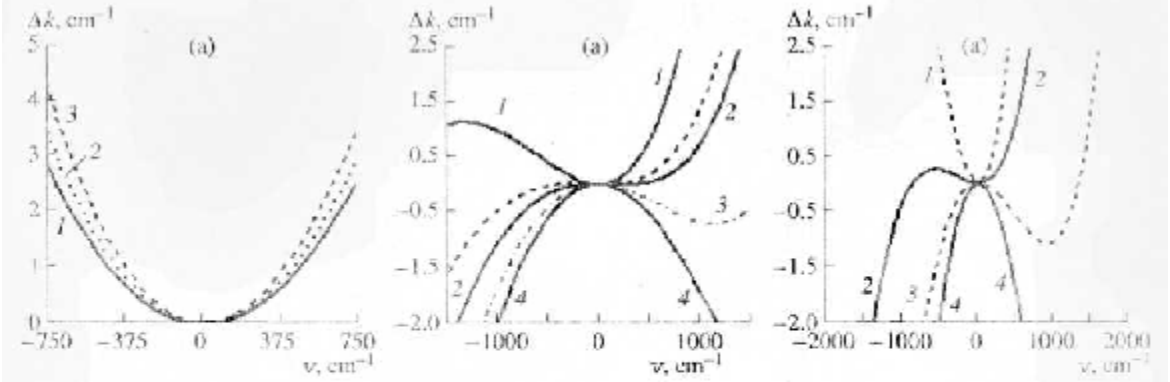

Fig. 4. Wavevector mismatch Δk versus $\nu = \Omega/2\pi c$ for a pump wavelength of 527 nm at various central wavelengths of the signal: a—KDP crystal at $\lambda_{10} = 1054$ nm (curve *1*), 1150 nm (*2*), and 1200 nm (*3*). b—DKDP crystal ($D = 0.96$) at $\lambda_{10} = 850$ nm (*1*), 911 nm (*2*), 950 nm (*3*), 1000 nm (*4*), DKDP crystal ($D = 0.84$) at $\lambda_{10} = 911$ nm (*5*). c—BBO crystal at $\lambda_{10} = 750$ nm (*1*), 800 nm (*2*), 850 nm (*3*), and 910 nm (*4*).

wave region), $\lambda_1 > \lambda_2$ (see Fig. 3a). Figure 3b shows that, in the DKDP crystal, the critical wavelength is $\lambda^*_{DKDP} = 1120$ nm, and the broadband phase matching in highly deuterated crystals at a pump wavelength of $\lambda_3 = 527$ nm occurs in the short-wavelength region of the signal $\lambda_{10} \le 1054$ nm. For the BBO crystal, the critical wavelength is $\lambda^*_{BB0} = 1430$ nm. At a pump wavelength of 527 nm in this crystal, the broadband phase matching exists in the short-wavelength region $\lambda_{10} < 1054$ nm (Fig. 3c).

Figure 4 shows the dependences of wavevector mismatch Δk on the value of frequency detuning $\nu = \Omega/2\pi c$ for several central wavelengths of the signal from the broadband phase-matching regions at a pumping $\lambda_3 = 527$ nm. It can be easily seen in Fig. 4a that, in the KDP crystal, for this pumping the value of the wavevector mismatch $\Delta k(\nu)$ is quadratically dependent on the frequency detuning, which corresponds to the case of broadband phase matching (Eqs. (4) and (5)). For the DKDP crystal (deuteration level 96%), the dependences $\Delta k(\nu)$ in the range $\lambda_1 < \lambda_2$ are illustrated in Fig. 4b. One can sec the dynamics of the quadratic parabola, which transforms into a cubic one as it enters the ultrabroadband phase-matching region ($\lambda_{10} = 910$ nm). In the ultrabroadband phase-matching region $\lambda_1 < \lambda_2$ for the BBO crystal at 527 nm pumping there is also a signal wavelength $\lambda_1 \sim 800$ nm that corresponds to the ultrabroadband phase matching (Fig. 4c).

Figure 5 shows the dependences of the gain coefficient of signal wave intensity $G(\nu)$ buildup by formula (1). In our calculations, we took into account that the value of pump intensity is limited by the threshold of the crystal resistance to damage by laser radiation and

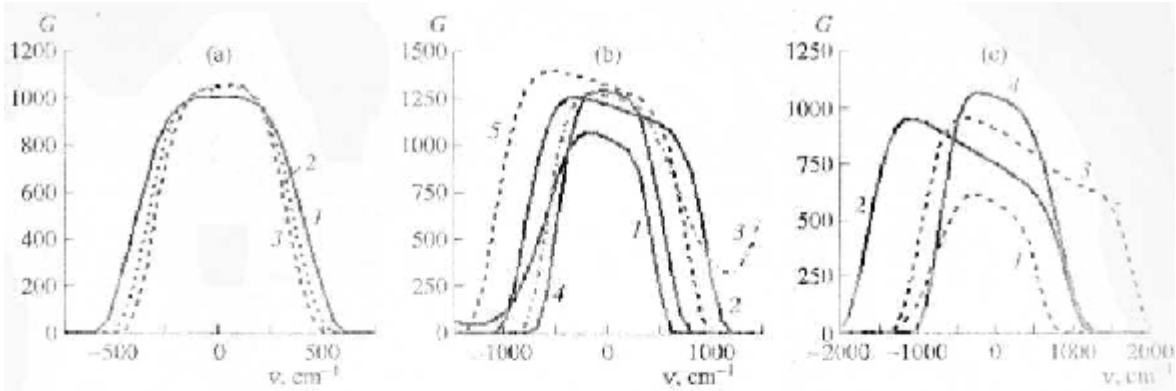

Fig. 5. Gain coefficient G versus frequency detuning of the signal wave $\nu = \Omega/2\pi c$ at a pump wavelength 527 nm at various central wavelengths of the signal λ_{10} for: a—KDP crystal ($L = 57$) at $\lambda_{10} = 1054$ nm (curve *1*), 1150 nm (*2*), and 1200 nm (*3*). b—DKDP crystal ($L = 68$, $D = 0.96$) at $\lambda_{10} = 850$ nm (*1*), 910 nm (*2*), 950 nm (*3*), 1000 nm (*4*), DKDP crystal ($D = 0.84$) at $\lambda_{10} = 910$ nm (*5*). c—BBO crystal ($L = 8$) at $\lambda_{10} = 750$ nm (*1*), 800 nm (*2*), 850 nm (*3*), and 910 nm (*4*).

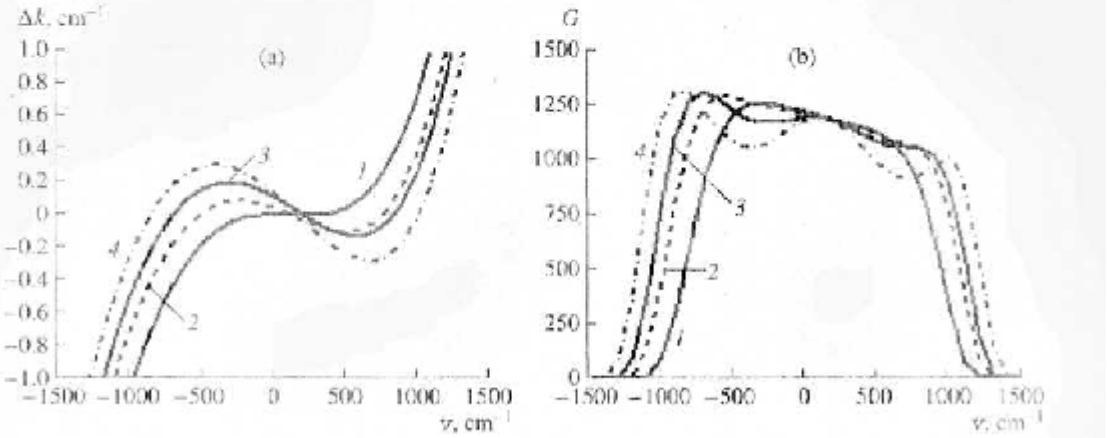

Fig. 6. Wavevector mismatch Δk and gain coefficient G of the signal wave in DKDP versus frequency detuning of the signal wave $\nu = \Omega/2\pi c$ at a pump wavelength of 527 nm for a central signal wavelength 911 nm. The different curves correspond to slight deviations of internal angles $\Delta\theta_3$ and $\Delta\varphi_{13}$ from the direction of fine broadband phase matching in a nonlinear element: 1—$\Delta\theta_3 = 0$ deg., $\Delta\varphi_{13} = 0$ deg.; 2—$\Delta\theta_3 = -0.02$ deg., $\Delta\varphi_{13} = -0.023$ deg.; 3—$\Delta\theta_3 = -0.03$ deg., $\Delta\varphi_{13} = -0.034$ deg.; 4—$\Delta\theta_3 = -0.045$ deg., $\Delta\varphi_{13} = -0.052$ deg.

chose the crystal length to provide identical amplitudes of the gain coefficient $G = 10^3$ and to have $L = 57$ mm (KDP), $L = 68$ mm (DKDP), and $L = 8$ mm (BBO). The dependences were calculated for pump intensity $I_3 = 1$ GW/cm^2 and coefficients of the matrix of nonlinear susceptibility [24] $d_{36} = 0.39$ pm/V (KDP), $d_{36} = 0.37$ pm/V (DKDP), $d_{22} = \pm 2.3$ pm/V, $d_{31} = \pm 0.16$ pm/V (BBO).

For the KDP crystal (Fig. 5a) at a pump wavelength of $\lambda_3 > \lambda^*_{KDP}/2$, the ultrabroadband phase-matching conditions (Eqs. (4)-(6)) are not fulfilled for any signal wavelengths, and the maximum gain bandwidth is achieved at degenerate phase matching. At the same time, for the short-wave pumping, for instance, $\lambda_3 = 450$ nm ($\lambda_3 > \lambda^*_{KDP}$), in KDP there is a central signal wavelength $\lambda_1 = 750$ nm at which the dependence $\Delta k(\nu)$ becomes cubic. At ultrabroadband phase matching, the gain bandwidth approximately twofold exceeds that near the degenerate interaction, and the absolute value of the gain coefficient of the signal intensity is several times greater [3].

Figure 5b presents the dependences of the gain coelfficient G(ν) in DKDP crystal (deuteration level 96%)

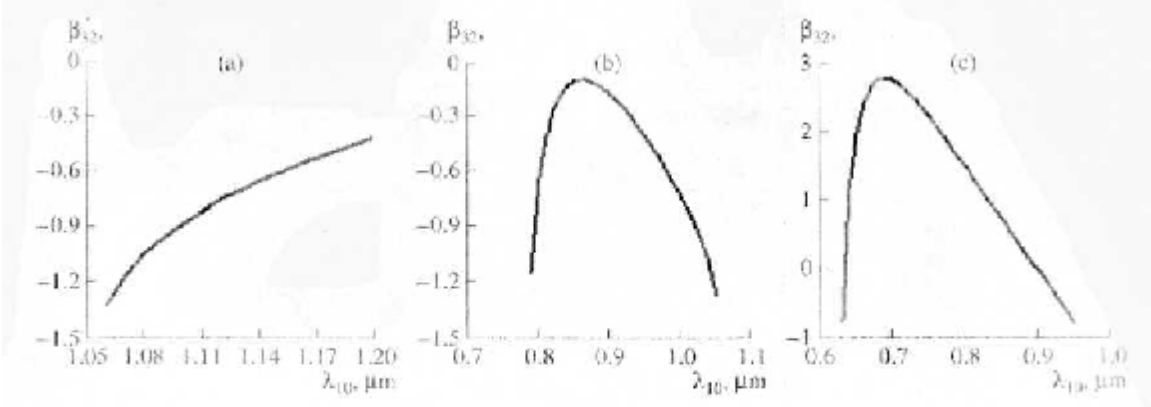

Fig. 7. Angle β_{32} between group velocities of pump and idler waves $\mathbf{V}_{G3}$ and $\mathbf{V}_{G2}$ versus signal wavelength λ_{10} when the broadband phase-matching condition is fulfilled for pump wavelength $\lambda_3 = 527$ nm: a—KDP crystal, b—DKDP crystal, c—BBO crystal.

for a pump wavelength of 527 nm. It can be seen that, near the point of ultrabroadband phase matching, the gain bandwidth of the signal considerably increases. The figure also shows that the effect of deuteration level on the gain bandwidth is insignificant for highly deuterated crystals.

Calculations for the BBO crystal showed that, for $\lambda_3 = 527$ nm, maximum gain bandwidth is achieved at a signal wavelength of ~800 nm (see Fig. 5c). At the same time, for a signal wavelength of ~910 nm, provided that the broadband phase-matching conditions (Eqs. (4) and (5)) are satisfied, the gain bandwidth is fairly large.

Note that the gain band of the optical parametric amplifier in the broadband and ultrabroadband phase-matching regions can be enlarged by optimizing the angle φ_{13} between the signal beam and the pump beam and the angle θ_3 between the pump direction and the crystal optical axis. It is seen from Fig. 6 that minor variations in the angles φ_{13} and θ_3 allow for modification of the shape of the dependence $\Delta k(\Omega)$ into an N-shape. thereby broadening the gain bandwidth of the signal wave [3].

To calculate parametric processes in nonlinear crystals, in addition to the characteristics considered above, it is important to know the direction of the group velocities of interacting waves. It is known that, if the group velocity directions of a pump wave $\mathbf{V}_{G3}$ and of an idler wave $\mathbf{V}_{G2}$ are close, then possible inhomogeneities of the spatial structure of pump radiation significantly affect the transverse structure of the idler; at the same time, the signal beam has a smoother transverse intensity distribution [29].

Figure 7 illustrates the dependences of the angle $\beta_{32}(\lambda_{10})$ between $\mathbf{V}_{G3}$ and $\mathbf{V}_{G2}$ when the broadband phase-matching condition is fulfilled in different crystals for a pump wavelength of $\lambda_3 = 527$ nm. Here, $\beta_{32} = \varphi_{32} - \beta$, $\varphi_{32} = \varphi_{12} - \varphi_{13}$, and β is the birefringence angle of the pump wave (see Fig. 1). Note that, for the KDP crystal (Fig. 7a), the values of the angle β_{32} are smaller far from the degenerate phase matching at $\lambda_{10} \sim 1200$ nm, which is nonoptimal for obtaining maximum gain band of the signal radiation. In contrast, for DKDP and BBO crystals in the $\lambda_{10} \sim$ 900-nm signal wavelength range, the idler and pump waves copropagate with a good accuracy, which is optimal for generating a high-quality spatial structure of the signal beam.

Summarizing the results of the preceding analysis of broadband amplification conditions at parametric type i interaction for KDP, DKDP, and BBO crystals, we can formulate the following two rules:

(i) The spectral range in which the broadband phase-matching conditions (Eqs. (4) and (5) are satisfied depends on the ratio between the doubled pump wavelength $2\lambda_3$ and the critical wavelength λ^*. For the pump radiation with a wavelength of $\lambda_3 > \lambda^*/2$, conditions (4) and (5) are fulfilled in the long-wavelength region of the signal, i.e., $\lambda_1 > \lambda_2$, and, at $\lambda_3 < \lambda^*/2$, they are fulfilled in the short-wavelength region: $\lambda_1 < \lambda_2$.

(ii) In the case of short-wavelength pumping ($\lambda_3 < \lambda^*/2$), there is a signal wavelength at which ultrabroadband phase-matching conditions (4)-(6) are fulfilled. In the case of long-wavelength pumping ($\lambda_3 > \lambda^*/2$), the ultrabroadband phase-matching condition is never fulfilled; the maximum gain bandwidth is obtained at degenerate three-wave interaction when $\lambda_1 = \lambda_2 = 2\lambda_3$.

An analysis of the data reported in [3] shows that these rules are valid for LBO as well.

Values of the parameters corresponding to broadband phase matching in the DKDP crystal for noncoilinear type I interaction $e(521) \rightarrow o(911) + o(1250)$, calculated by two close Sellmeier equations, and several experimentally measured values at which the broadband optical parametric amplification is provided are summarized in Table 1.

1.4. Comparison of KDP and DKDP Crystals

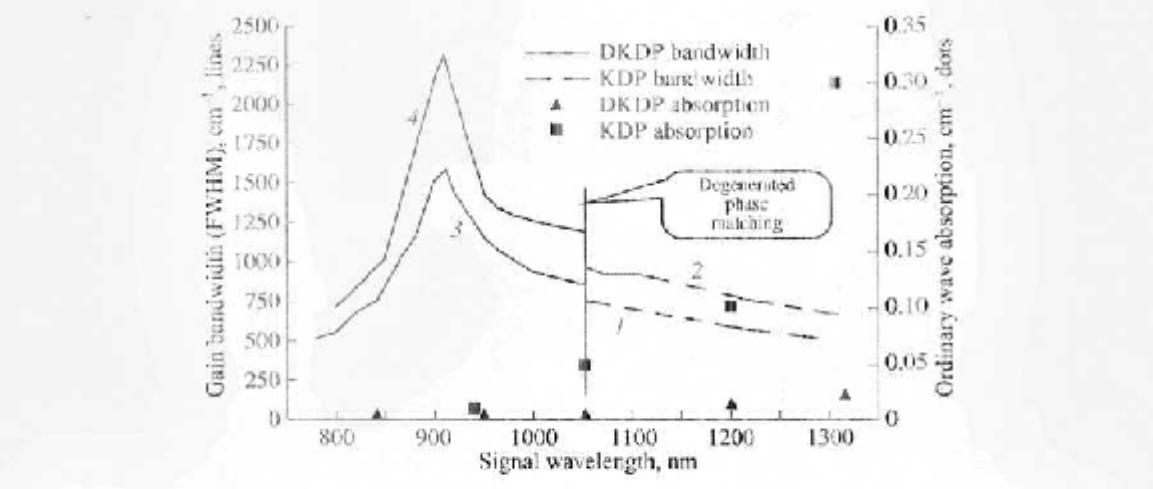

Fig. 8. Ordinary wave absorption [24] and gain bandwidth (FWHM) versus its wavelength at pump intensity 1 GW/mm^2, pump wavelength λ_3 = 527 nm, and length of the nonlinear medium 70 mm: 1—KDP crystal when the broadband phase-matching condition is fulfilled, 2—same at optimized angles; 3—DKDP crystal when the broadband phase-matching condition is fulfilled, 4—same at optimized angles.

Figure 8 shows calculated dependences of the bandwidth of the signal on its wavelength for KDP and DKDP crystals at interaction angles at which the broadband phase-matching condition for KDP and DKDP crystals is satisfied and for the case of optimized angles at a pump wavelength of 527 nm.

In the KDP crystal, the maximum gain bandwidth ~1000 nm^{-1} is obtained near degenerate collinear phase matching at a signal wavelength of 1054 nm [3], where no lasers with the pulse duration required for the creation of petawatt lasers (30 fs and shorter) are available. In the DKDP crystal, the maximum bandwidth ~2300 nm^{-1} is obtained in the noncollinear interaction scheme at a signal wavelength of 911 nm and a wavelength of the conjugated (idler) wave of 1250 nm. This considerable difference in gain bandwidths of the crystals is due to the fact that, in DKDP, ultrabroadband phase-matching conditions (7) can be fulfilled when, in the wavevector mismatch, not only zero and linear terms but also the quadratic term become zero. Ti:sapphire and Cr:forsterite lasers, the sources of femtosecond pulses, operate at these wavelengths, namely, at 910 nm and 1250 nm, respectively [30, 31].

An important point worth mentioning here is that, when the broadband signal is amplified, the idler wave is strongly dispersed, as boundary conditions (2) require. For the external angle between the signal and idler waves (Fig. 1), the wavelength dependence is almost linear and is given by the expression

$$\psi_{12}(\lambda_2) \approx \sin\psi_{12}(\lambda_2) = \frac{k_{3z}}{2\pi}\lambda_2 = \text{const}\,\lambda_2. \qquad (10)$$

However, if the injected radiation with the central wavelength of 1250 nm follows the linear law of angular dispersion (10), the broadband radiation excited a optical parametric amplification with a central wave length of 911 nm will be collimated. This circumstance provides an additional degree of freedom when creating an OPCPA system. Femtosecond Cr:forsterite laser oscillate at a wavelength of 1250 nm, so it would b reasonable to use their? as a source of broadband radiation to be injected into the nonlinear DKDP crystal f se Section 3).

Another obvious advantage is that there is almost гь linear absorption in the DKDP crystal as compared *u* KDP at optimal signal wavelengths for these crystal [24] (see Fig. 8).

At a pump wavelength of 527 nm, the BBO crystal also has a broad gain bandwidth in the ultrabroadband phase-matching region in DKDP (911 nm) (Fig. 5c) The effective nonlinearity in BBO is almost one order of magnitude higher than in DKDP; therefore, a lengl[1] of the BBO nonlinear element of one order of magnitude smaller is needed to obtain the same gain coefficient as in the DKDP crystal. Thus, the BBO crystal can be efficiently exploited in preamplification stages o multiterawatt and petawatt systems, with the DKDP crystal used in the final states

2. EXPERIMENTAL INVESTIGATION OF BROADBAND OPCPA IN DKDP CRYSTAL

In the previous section, we discussed theoretical aspects of optical parametric amplification of a broad band collimated signal. To verify the theoretical computations and determine the conditions for broadband amplification in the DKDP crystal, it is important to measure experimentally a family of tuning characters-

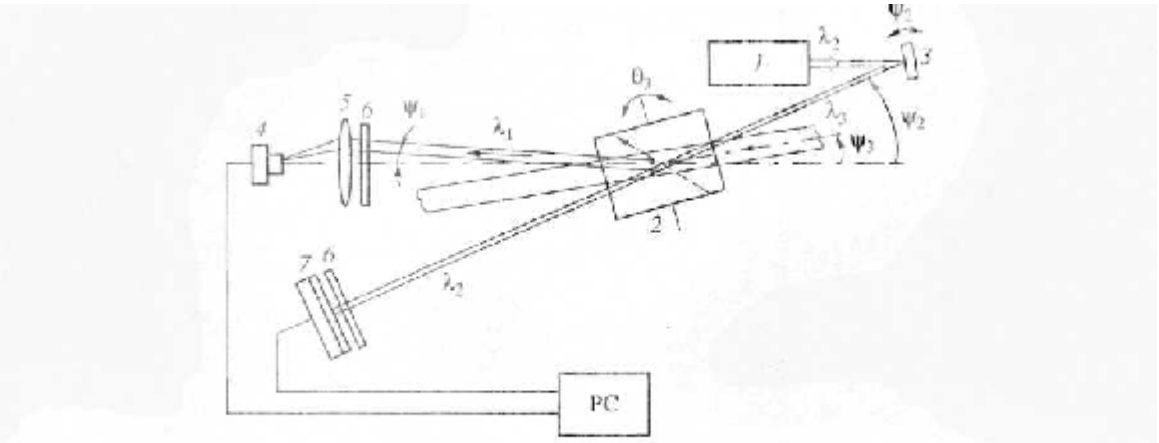

Fig. 9. Layout of the experiment: *1* — Cr:forsterite laser, *2* — DKDP crystal, *3* — mirror, *4* — CCD camera, *5* — lens, *6* — filter, *7* — photodiode array.

tics, i.e., the dependences of the angles $\varphi_{13}(\lambda_{10})$ and $\varphi_{23}(\lambda_{20})$ on the angle θ_3 at fine phase matching:

$$\mathbf{k}_3 = \mathbf{k}_1(\lambda_{10}) + \mathbf{k}_2(\lambda_{20}).$$

Our interest in these dependences is due to the following aspects. It is difficult to measure directly the dependence $\Delta k(\Omega)$ experimentally. At the same time, the angle $\varphi_{13}(\lambda_{10})$ is determined by the relation

$$\cos\varphi_{13}(\lambda_{10}) = \frac{k_3^2 + k_1^2(\lambda_{10}) - k_2^2(\lambda_{20})}{2k_1(\lambda_{10})k_3}.$$

By differentiating this relation, we can easily show that, if broadband phase-matching conditions (4) and (5) are fulfilled for some values of λ_{10}, φ_{13}, and θ_3, then $\frac{d\varphi_{13}}{d\lambda_{10}} = 0$, while, if ultrabroadband phase-matching conditions (4)–(6) are fulfilled, the second derivative becomes zero as well: $\frac{d^2\varphi_{13}}{d\lambda_{10}^2} = 0$. Therefore, the form of the tuning curve $\varphi_{13}(\lambda_{10})$ for a certain value of θ_3 allows one to judge the character of the dependence $\Delta k(\Omega)$ for the same values of λ_{10} and θ_3.

Note that the presence of a horizontal region in the tuning characteristic being measured for the external angle $\psi_{13}(\lambda_1)$ suggests that the angle θ_3 was adjusted correctly, and the angular dispersion of the injected wave necessary to obtain a collimated signal can be found by the slope of the dependence $\psi_{23}(\lambda_2)$ (see expression (10)).

A schematic layout of the experiment is shown in Fig. 9. Radiation at $\lambda_2 = 1250$ nm from a femtosecond laser (*1*) was injected into a DKDP crystal (*2*), and the phase-matching angle ψ_2 was adjusted by rotating a mirror (*3*). To enhance the measurement accuracy of the phase-matching parameters, the experiment was conducted at a low pump intensity $I_3 \sim 1$—10 MW/nm^2, where the width of the dependence of the gain coefficient G (Eq. (1)) on wavevector mismatch Δk is minimal. The pump pulse duration was increased up to 15 ns to reliably register the signal; the energy was varied within 5-120 mJ. To increase the spectral brightness, the injecting femtosecond laser operated in the continuous-wave regime with an average power of ~300 mW, and its wavelength was tuned throughout the experiment within 1210-1280 nm. The spectral line width of generation was several fractions of a nanometer, and the wavelength was controlled to an accuracy of ±1 nm. The energy of the injected radiation cutoff by the pump pulse duration was 2.5 nJ in the band center ($\lambda_{2c} = 1250$ nm) and decreased by approximately one order of magnitude in the limits of the detuning range. The signal beam was focused onto camera (*4*) by a lens (*5*) with a focal length $f = 133$ mm. Therefore, the camera registered angle ψ_1 of the signal radiation. Pump radiation and background radiation were cut off by light filters (*6*). A photodiode array (*7*) was used to register the injected wave and to measure the external angle ψ_2. The experimental accuracy of the angle measurements was ±1 angular minute.

The measured values of the central angles of the phase matching for two deuteration levels, namely, 89 ± 0.3% and 84 ± 2% [12. 32], are summarized in Table 1. Figure 10 presents experimentally obtained tuning characteristics of fine phase matching in DKDP ($D = 0.89 \pm 0.005$) and theoretical curves calculated by formula (8) for the two closest Sellmeier equations (see Table 1).

It is seen from Fig. 10a that curve $\psi_{13}(\lambda_1)$ has a horizontal region corresponding to broadband phase matching. The experimental accuracy of these measurements was ±0.5 angular minute. Curve $\psi_{23}(\lambda_2)$

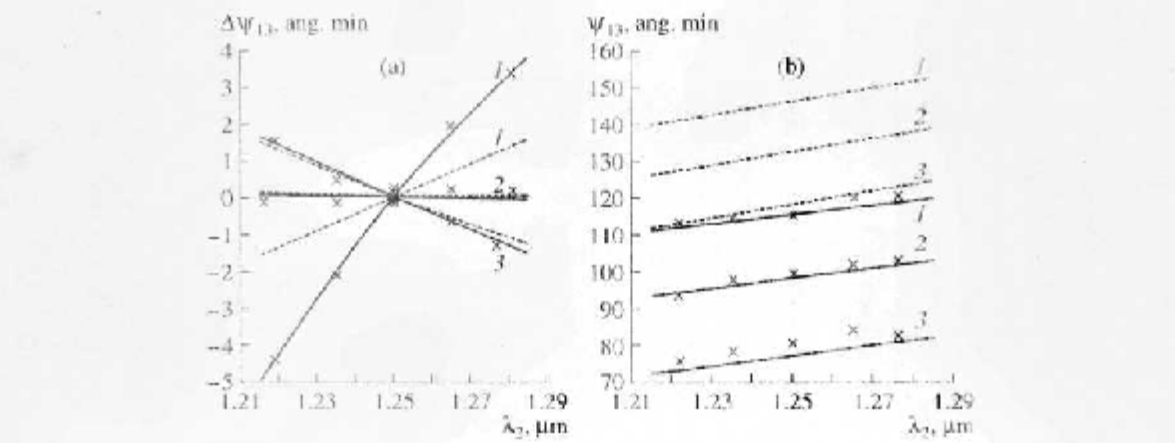

Fig. 10. Tuning curves for external angles at various values of θ_3 for DKDP ($D = 0.89$): theoretical curves for modified (solid line) and standard (dotted line) Sellmeier equation [18], calculated by formula (8), and experimental data (spots). a) dependences $\Delta\psi_{13} = \psi_{13}(\lambda_2) - \psi_{13}(\lambda_{20})$ at $\Delta\theta_3 = -23$ ang. min (*1*), 0 (*2*), +34.5 (*3*) b) dependences ψ_{23} on λ_2 at $\Delta\theta_3 = 110$ ang. min (*1*), 0 (*2*), −110 (*3*).

(Fig. 10b) shows the angular dispersion of the injected idler wave. The plots demonstrate a good agreement between the experimental results and theoretical calculations by dependence (9) at least for highly deuterated DKDP crystals.

The theoretical results were also experimentally confirmed in the study of parametric superluminescence. A contrasted cone of parametric superluminescence is seen in the far field (Fig. 11), suggesting the presence of broadband phase matching at a given angle 9_3. The coincidence of the phase-matching angle of the signal wave (λ_{1c} = 911 nm) with the superluminescence cone at injection of the idler wave with λ_{2c} = 1250 nm indicates that the frequency of the signal gels into the broadband phase-matching band.

The tuning characteristic $\psi_{13}(\lambda_1)$ can be found by measuring the frequency-angular spectrum o Γ the parametric superluminescence. Figure 12 shows a family of tuning characteristics depending on parameter θ_3, which were obtained by superimposing images of the directional diagram of parametric superluminescence. The horizontal characteristic corresponds to broadband phase matching in the DKDP crystal.

We also studied the dependence of the propagation direction of the spectral components of the amplified signal on the angular dispersion coefficient $d\psi_2/d\lambda_2$

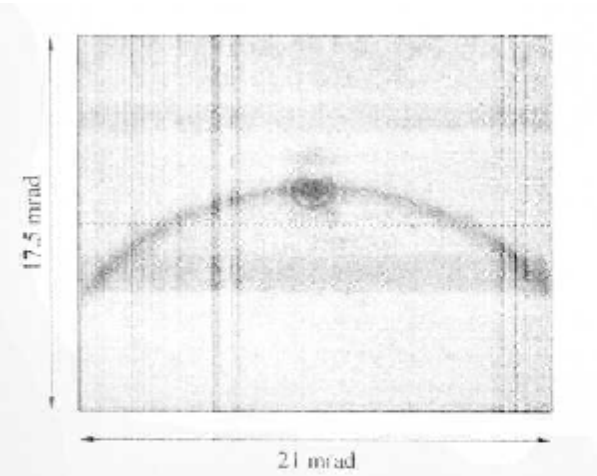

Fig. 11. The far field of the signal and the cone of parametric superluminescence.

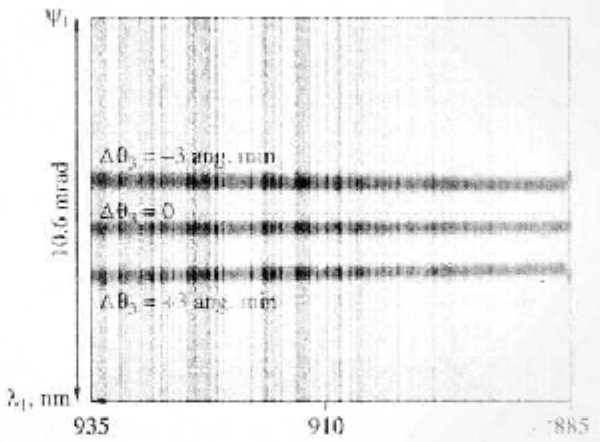

Fig. 12. Spectral diagrams of parametric superluminescence when parameter θ_3 is changed with a step of 3 angular minutes.

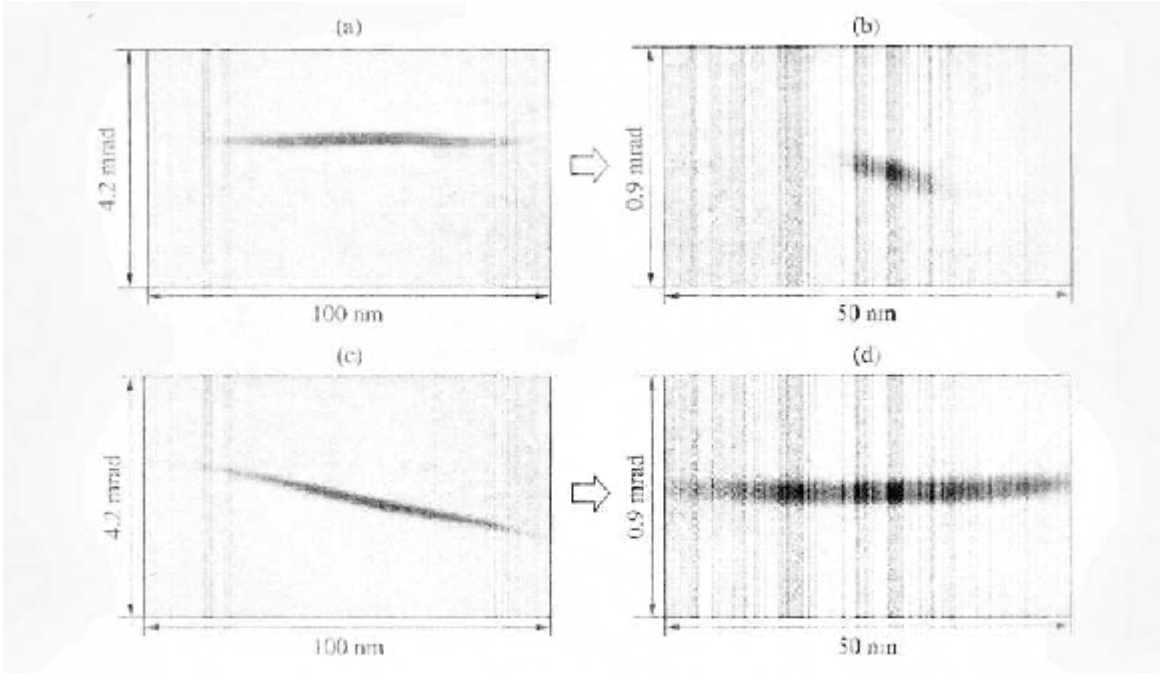

Fig. 13. Spectral dependences of the directional diagram in the critical plane in the lens focus $f = 406$ mm of: a, c—injected radiation at $\lambda_{20} = 1250$ nm (a—collimated radiation, c—at optimal angular dispersion); b, d—signal radiation at $\lambda_{10} = 911$ nm. Note that angular scales on the left and right figures differ.

(Table 1) of the injected radiation [13, 32]. When a collimated beam ($\lambda_{20} = 1250$ nm) was injected into a parametric converter, the output signal radiation ($\lambda_{10} = 911$ nm) is angle-dispersed (Fig. 13a). When we used a specially made prism providing the required dispersion, the signal beam became collimated, and the signal spectrum considerably broadened (Fig. 13b).

Based on this experimental fact, we excluded from consideration the Sellmeier equations from [20, 22], which, for 527-nm pumping, predicted broadband phase matching for a long-wavelength signal ($\lambda_{10} \geq 1054$ nm).

Thus, all the results obtained experimentally (see Figs. 10-13 and Table 1) indicate that Sellmeier formula (9) most correctly describes the properties of the DKDP crystal and provides the best agreement between the calculated and measured values.

3. A 0,4-TW LASER BASED ON OPCPA IN DKDP

Based on the results described in the above discussion, we designed a DKDP-based laser system with OPCPA. The laser (Fig. 14) comprises a pump system, a chirped pulse injection system, a three-stage optical parametric amplifier, a compressor, and an electronic system for laser synchronization, which allowed for simultaneous propagation of pump pulses and amplified radiation into the nonlinear crystals [33].

The injection system comprises a femtosecond source, a stretcher, beam-matching telescopes, and a prism made of K-8 (BK-7) glass with a vertex angle of 40 degrees to impart a corresponding angular dispersion to the injected radiation. The source of the injected radiation is a femtosecond Cr:forsterite laser with an average power of ~0.25 W, which generates pulses with duration ~40 fs and spectral width -400 nm^{-1} (FWHM). The stretcher, with a bandwidth 1000 nm^{-1}, stretches pulses up to 0.6 ns and introduces negative third-order dispersion. thereby ensuring compression of the pulse with a wavelength of 911 nm [12].

The optical parametric amplifier is pumped by the second harmonic of a single-mode single-frequency Nd:YLF laser with a wavelength of 527 nm, pulse energy up to 1 J, and pulse duration 1.5-1.7 ns. The pulse repetition rate was 2 Hz. The intensity of the pump pulse with a radius of 5 mm at the input of the optical parametric amplifier bad a nearly uniform transverse distribution and was ~1 GvV/nm^2

The three-stage optical parametric amplifier consists of a two-pass amplifier OPA (*1*) and a single-pass amplifier OPA (*2*). The two-stage optical parametric amplifier [32] performs broadband conversion of chirped pulses at a conjugated wavelength $\lambda_{20} = 1250$ nm into pulses of signal radiation ($\lambda_{10} = 911$ nm) and amplifies them in the field of intense pumping. To weaken the effect of pump pulse divergence on the con-

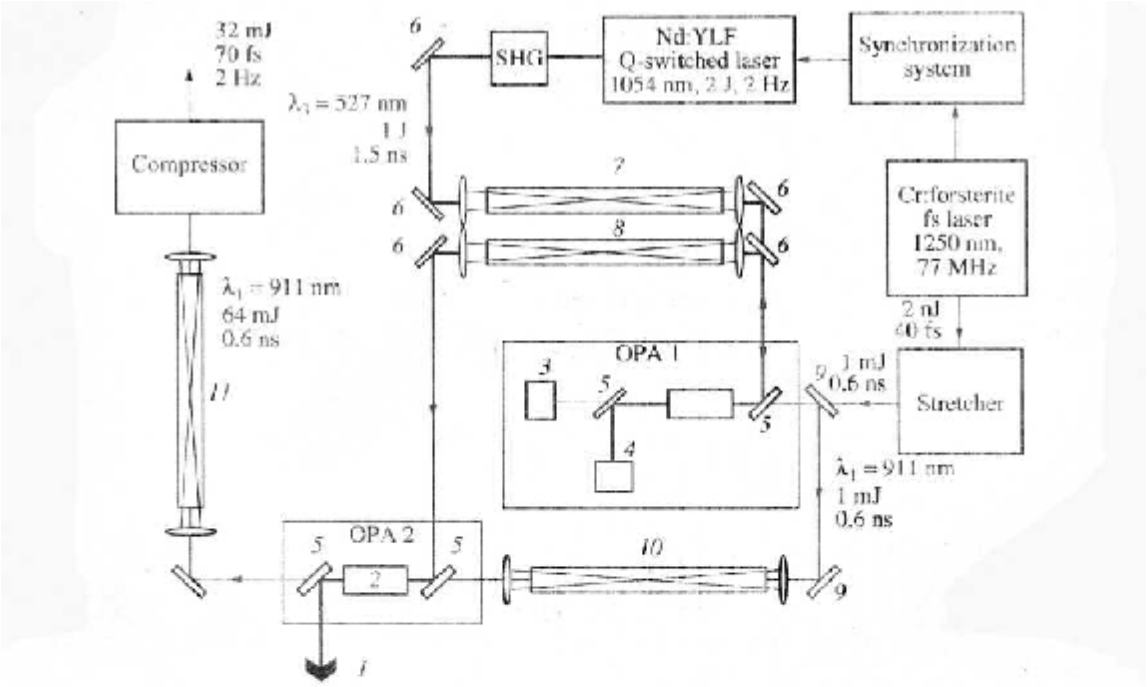

Fig. 14. Optical layout of the laser system: *1*, *2*—nonlinear DKDP elements; *3*—corner reflector of signal wave; *4*—roof prism; *5*—dichroic mirrors; *6*—pumping mirror; *7*, *8*—pump image transformers; *9*—signal mirror; *10*, *11*—telescope with spatial filter of signal beam; *12*—beam block.

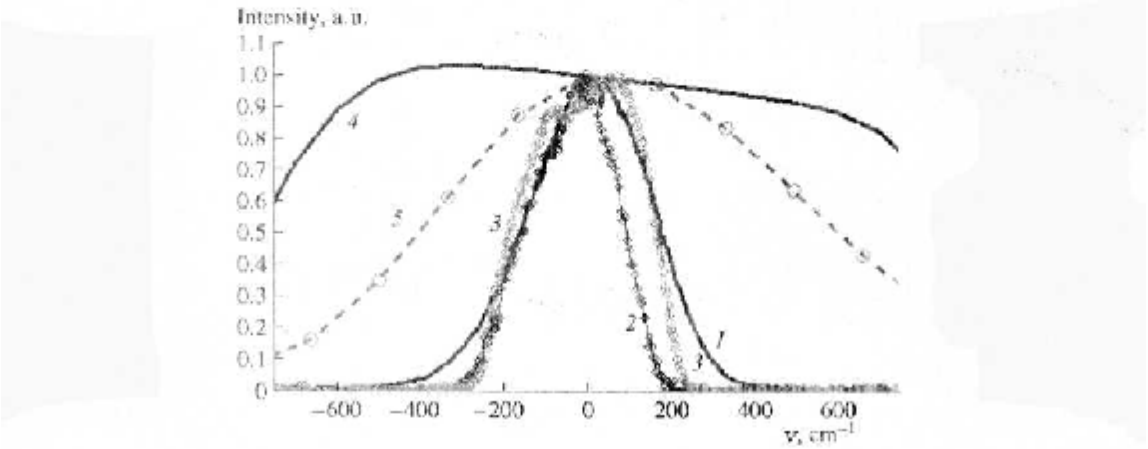

Fig. 15. Spectral dependences on frequency detuning of *1*—injected radiation with $\lambda_{20} = 1250$ nm, *2*—signal amplified in OPA2 with $\lambda_{10} = 911$ nm, *3*—signal at the output from OPA2 at saturation, *4*—parametric gain in DKDP crystal, and *5*—pump intensity in which the corresponding spectral components of signal are amplified.

version process, the radius of the injected beam was ~1 mm. The second stage of OPA1 broadband amplification of collimated signal radiation was performed at the same phase-matching parameters as in the first OPA stage, owing to the corner reflector, which reflects the signal, and the roof prism, which reflects the pump. This makes the adjustment of OPA 1 much easier.

On the experimental setup, we investigated the spectral-angular characteristics of ultrabroadband phase

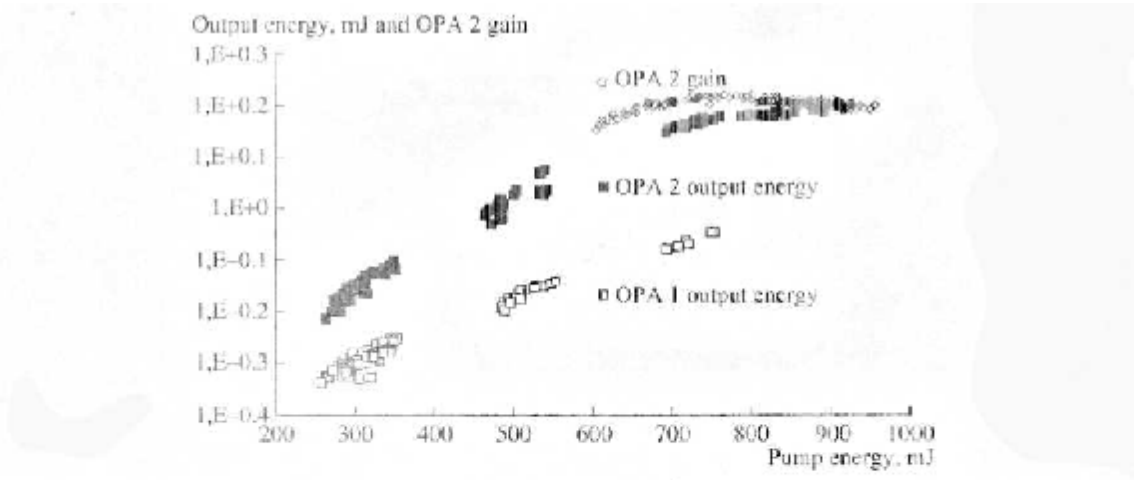

Fig. 16. Output energy in OPA1 (open squares), OPA2 (closed squares) and gain coefficient of OPA2 (circles) versus pump energy.

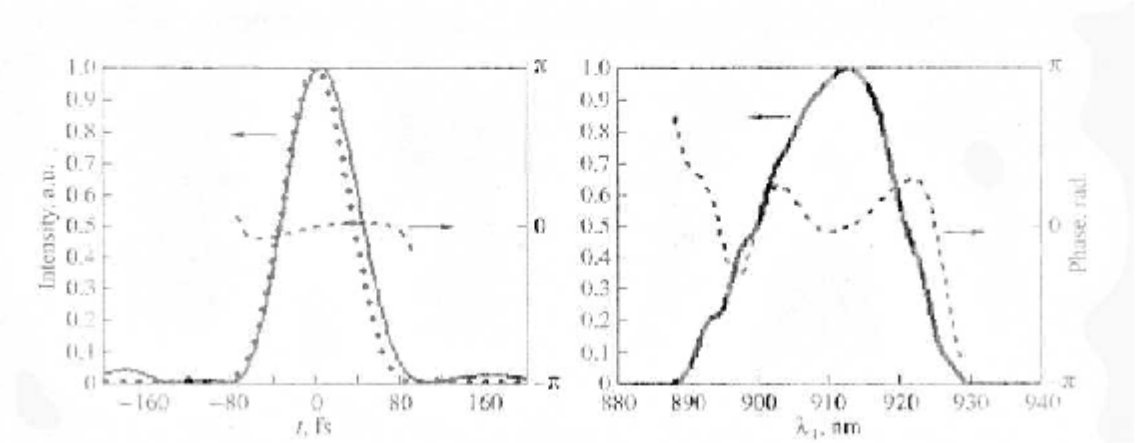

Fig. 17. SPIDER reconstruction of compressed pulse: a — temporal profile (solid), residual phase (dashed) of the pulse and theoretical Fourier limit (dotted) for intensity of the measured spectrum, b — pulse spectrum (solid) and residual phase (dashed).

matching and the spatial, energy, and temporal parameters of signal radiation.

The measurements showed a good agreement between the spectra of the injected idler and amplified signal in OPA2 radiation for linear amplification (Fig. 15). Slight narrowing of the spectrum under amplification results from a nonrectangular shape of the pump pulse.

A third stage of optical parametric amplification in OPA2 operating in the regime of saturated amplification was used to efficiently convert pump energy into the signal wave [12]. Figure 16 illustrates the dependences of pulse energy at the output of OPA1 and OPA2 and the gain coefficient of OPA2 on pump energy.

In the nonlinear amplification regime, the intensity of wings of the signal pulse grew faster than its central part; as a result, the spectral width increased (Fig. 15). This effect was also observed in [34]. Pulses with duration ~70 fs were generated upon signal compression without fine adjustment of the stretcher—compressor system [14, 15]. The pulse duration was measured by means of a SPIDER [35] made by Avesta Project Ltd. The reconstructed pulse and spectrum and the theoretical Fourier limit are shown in Fig. 17. The pulse energy at the output of the compressor was 30 mJ.

The results of numerical modeling show that the 100-TW power level can be achieved by adding one more OPA. 100 mm in diameter with a pump energy of 70 J.

CONCLUSION

Based on the experiments we performed and the comparison of the results with our theoretical analysis

and the literature, the following main results can be formulated.

7'he validity of data on the Sellmeier formula [18] with modification (9) has been confirmed experimentally. The broadband optical parametric chirped pulse amplification conditions in the DKDP crystal pumped by the second harmonic of a Nd:YLF laser have been investigated. Specifically, the spectral-angular characteristics of ultrabroadband nondegenerate phase matching have been studied for a 911-nm signal in a DKDP crystal.

It is shown that the DKDP crystal is more suitable than the KDP crystal for powerful OPCPA stages in petawatt lasers. In addition, both the DKDP and BBO may be used for the first stages of amplification.

A laser with a power of 0.4 TW at a wavelength of 911 nm has been created, which is based on a Cr:forsterite laser and optical parametric amplification in the DKDP crystal. Taking into account the scaling possibility, the creation of a multipetawatt femtosecond laser based on OPCPA in the DKDP crystal looks very promising.

REFERENCES

1. A. Piskarskas, A. Stabinis. and A. Yankauskas, USp. Fiz. Nauk 150, 127 (1986) [Sov. Phys. Usp. **29**, 869 (1986)].
2. A. Dubietis, G. Jonusauskas, and A. Piskarskas, Opt. Commun. **88**, 437-440 (1992).
3. I. N. Ross, P. Matousek, M. Towrie, *et ah.* Opt. Commun. **144**, 125-133(1997).
4. P. Matousek. B. Rus, and 1. N. Ross, IEEE J. Quantum Electron. **36**, 158-163 (2000).
5. J, Collier, C. I lernandez-Gomez, I. N. Ross, *et ah,* Appl. Opt. **38**, 7486-7493(1999).
6. I. N. Ross, J. L. Collier, P. Matousek, *et ah,* Appl. Opt. **39**, 2422-2427 (2000).
7. 1. Jovanovic, B. J. Comaskey, C A. Ebbers, *et ah,* in *Proceedings of the Conference on Lasers and Electro-Optics (CLEO), CPD8-1-2, OSA Trends in Optics and Photonics, 2001* (Optical Society of America, Washington, 2001).
8. 11. Yoshida, E. Ishii, K. Sawai, *et ah,* in *Proceedings of the Conference on Lasers and Electro-Optics (CLEO), 99-100] OSA Trends in Optics and Photonics, 2001* (Optical Society of America, Washington, 2001).
9. 1. N. Ross, P. Matousek, and J. L. Collier, in *Proceedings of the Conference on Lasers and Electro-Optics (CLEO), 99-100, OSA Trends in Optics and Photonics, 2001* (Optical Society of America, Washington, 2001), p. 249.
10. S. K. Zhang, M. Fujita, H. Yoshida, *et ah,* in *Proceedings of the Conference on Lasers and Electro-Optics (CLEO), 99-100, OSA Trends in Optics and Photonics, 2001* (Optical Society of America, Washington, 2001), pp. 249 250.
11. X. Yang, Z. Xu, Z. Zuakg, *et ah,* Appl. Phys, B **73**, 219-222 (2004).
12. N. F. Andreev, V. I. Bespalov, V. I. Bredikhin, *et ah,* Pis'ma Zh. Eksp. Teor. Fi. **79**, 178 (2004) | JETP Lett. 79, 144(2004)].
13. G. Freidman, N. Andreev, V. Bespalov, *et ah,* in *Proceedings of the Conference on Lasers and Electro-Optics (CLEO), CPDA9-1, 2002.*
14. V. I. Bespalov, V. I. Bredikhin. G. I. Freidman, *et ah,* in *Proceedings of Conference on Lasers and Electro-Optics (CLEO), IQEC2004,* CD-ROM.
15. K. L. Dvorkin, V, N. Ginzburg, G. I. Freidman, *et ah,* in *Proceedings of the International Symposium on Modern Problems of Laser Physics, Novosibirsk, Russia, 2004* (ILP, Novosibirsk, 2004) p. 118.
16. http://www.clevelandcrystals.com/news.shtml.
17. X. Yang, H.-Z. Z. Xu, Y.-X. Leng, *et ah,* Opt. Lett. **27**, 1135-1137(2002).
18. K. W. Kirby and L. G. DeShazer, J. Opt. Soc. Am. B **4**, 1072-1078(1987).
19. R. A. Phillips. J. Opt. Soc, Am. **56**, 629-632 (1966).
20. G. C. Ghosh and G. C. Bhar, IEEE J. Quantum Electron. **QE-18**, 143(1982).
21. V. I. Bredikhin and S. P. Kuznetzov, Opt. Spektrosk. **61**, 103-107 (1986) [Opt. Spectrosc. **61**, 68-72 (1986)].
22. E. N. Volkova and S. L. Faerman, Kvantovaya Elektron, **6**, 1380(1976).
23. http://www.castech.com /doce/cp-dkdp.htm.
24. V. G. Dmitriev, G. G. Gurzadyan, and D. N. Nikogosyan, *Handbook of Nonlinear Optical Crystals,* 3rd ed. (Springer, Berlin, i 999).
25. F. Zernike, J. Opt. Soc. Am. **54**, 1215 - 1220 (1964).
26. F. Zernike, J. Opt. Soc. Am. **55**, 21O(E) (1965).
27. M.S.Webb,D.Eimerl,andS.P.Velsko,J.Opt.Soc.Am. B **9**, 1118-1127(1992).
28. K. Kato, IEEE J. Quantum Electron. **22**, 1013 1014 (1986),
29. A. A. Babin. N. N. Belyaeva, Y. N. Belyaev, and G. I. Freidman, Zh. Eksp. Teor. Fiz. **71**, 97-110 (1976) [Sov. Phys. JETP **44**, 50--57 (1976)].
30. A. Seas, V. Petricevic, and R. R. Alfano, Opt. Lett. **17**, 937(1992).
31. V. Yanovsky, Y. Pang, F. W. Wise, and B.I. Minkov, Opt. Lett. **18**, 1541 (1993).
32. G. Freidman, N. Andreev, V. Bespalov, *et ah,* Proc. SPIE **4972**, 13(2003).
33. E. V. Katin, E. A. Khazanov, V. V. Lozhkarev, and O. V. Palashov, Kvantovaya Elektron. **33**, 836 (2003).
34. I. Jovanovic, C. A. Ebbers, B. C Stuart, *et ah,* in *Proceedings of the Conference on Lasers and Electro-Optics (CLEO), OSA Trends in Optics and Photonics, 2002* (Optical Society of America. Washington, 2002), pp. 38^-388.
35. C. Iaconis and LA. Walmsley, Opt. Lett. **23**, 792 (1998).